

# Methane Gas Hydrates Viewed through Unified Solid–Liquid–Vapor Equations of State

A. Yokozeki<sup>1</sup>

*Received March 1, 2004*

---

The phase behavior of methane gas hydrates (clathrates) has been investigated with unified equations of state for solid–liquid–vapor phases. This is a new way to look at the clathrate-containing system, being radically different from the traditional statistical thermodynamic model for clathrates. The present paper includes modifications and refinements of the previously published method with the unified equations of state. The univariant three-phase equilibrium lines containing clathrates have been successfully predicted with the present equation-of-state model for a wide temperature and pressure range. Particularly, the phase behavior in very high-pressure regions has been modeled for the first time by the present work. Although the present results at high pressures are still tentative, they will shed some light on the unsettled problem of high pressure phases as reported in the literature.

---

**KEY WORDS:** clathrate; equation of state; gas hydrate; methane; modeling; phase equilibrium; solid–liquid–vapor; univariant state; water.

## 1. INTRODUCTION

Gas hydrates are water ices that contain “guest” gaseous molecules inside the ice cavity, and can be formed even above the melting temperature of the pure water ice. This curious “ice” (hydrate) formation has long been a problem in natural gas production and transportation by plugging gas pipelines, and numerous related articles have been published. However, the recent impetus of hydrate research has been toward the use of its unique state of matter: a potential energy source of a large amount of methane hydrates deposited in the ocean floor [1, 2], ocean sequestration of

---

<sup>1</sup>DuPont Fluoroproducts Laboratory, Chestnut Run Plaza 711, Wilmington, Delaware 19880, U.S.A. E-mail: akimichi.yokozeki@usa.dupont.com

ever-increasing carbon dioxide as gas hydrate [3, 4], cooling storage material [5], desalinization of sea water [6], *etc.* Thus, an accurate knowledge and understanding of the phase behavior of the clathrate state are highly desired for these engineering applications.

So far, modeling of the clathrate-hydrate phase equilibria has been based on statistical thermodynamics by van der Waals and Platteeuw [7], although there have been many improvements and extensions of the original work [8–15]. However, recently we have proposed a completely new method to model the phase behavior of clathrate-containing systems [16]. The new method is to use a unified equation of state (EOS) for solid, liquid, and vapor states in a thermodynamically consistent way. In this report, we have made some improvements on the proposed method and applied it to the methane gas hydrate system.

The organization of the text is as follows. First, the unified solid–liquid–vapor EOS [17] is briefly presented for pure water and methane. This is followed by discussion of the mixture EOS and how to model the clathrate state with the present EOS. In Section 3, the overall result of the univariant three-phase behavior of methane gas hydrates is first shown for a wide range of temperature and pressure conditions. Then, the detailed analyses and results follow with three separate pressure regions: medium, low, and high pressures. The complex behavior and the unsettled problem in the literature [18–21] at high pressures are discussed, as well as the advantage of the present model in Section 4. Finally, concluding remarks of the present work are given.

## 2. THERMODYNAMIC MODEL

In this section, we first summarize our unified solid–liquid–vapor EOS [17] for pure compounds, and then describe the mixture EOS, followed by the clathrate-state model within the present EOS method.

### 2.1. Pure Compound

A pure compound EOS is the following unified solid–liquid–vapor EOS [17]:

$$P = \frac{RT}{V-b} \left( \frac{V-d}{V-c} \right) - \frac{a}{V^2}, \quad (1)$$

where the parameters,  $a$ ,  $b$ ,  $c$ , and  $d$ , are given by

$$a = a_r \frac{(RT_c)^2}{P_c}, \quad b = b_r \frac{Z_c RT_c}{P_c}, \quad c = c_r \frac{Z_c RT_c}{P_c}, \quad d = d_r \frac{Z_c RT_c}{P_c} \quad (2)$$

where  $R$  is the universal gas constant,  $P_c$  is the critical pressure,  $T_c$  is the critical temperature, and  $Z_c$  is the critical compressibility factor.

The EOS constants in Eq. (2) are given in Table I for methane and water except for  $a_r$  and  $b_r$ . The temperature-dependent parameters  $a_r$  and  $b_r$  for each pure compound are modeled by [17]

$$a_r(T_r) = a_0 + a_1 T_r \exp(-a_2 T_r^n), \quad (3)$$

$$b_r(T_r) = b_0 + b_1 \exp(-b_2 T_r^m), \quad (4)$$

where  $T_r$  is a reduced temperature,  $T/T_c$ . The constants in both equations for methane and water are listed in Table II. The procedure to determine the constants in Tables I and II is given in Ref. 17. In the present study, however, we used an additional data point (saturated vapor pressure at  $T_r = 0.7$ ) in order to improve the vapor pressure representation. Figures 1 and 2 show phase diagrams which were calculated with the present EOS constants.

## 2.2. Mixture

The EOS for mixtures is the same as Eq. (1), except that the EOS constants are constructed by proper “mixing” rules. For the attractive part of the EOS parameter for mixtures, we use the “van Laar type” of mixing rule, which is often successfully applied for highly non-ideal systems [16, 22, 23], and justifications for such a mixing rule are discussed in Ref. 22.

**Table I.** EOS Constants of Pure Compounds Used in the Present Model<sup>a</sup>

	$c_r$	$d_r$	$Z_c$	$T_c$ [K]	$P_c$ [MPa]
Water	0.33790	0.33022	0.37503	647.1	22.064
Methane	0.34307	0.33845	0.37504	190.56	4.5992

<sup>a</sup>Coefficients in Eq. (2).

**Table II.**  $T$ -dependent EOS Constants of Pure Compounds Used in the Present Model<sup>a</sup>

	$a_0$	$a_1$	$a_2$	$n$	$b_0$	$b_1 (\times 10^{-3})$	$b_2$	$m$
Water	0.17432	8.7883	3.5698	0.75	0.3255	-5.2129	5.61866	6
Methane	0.35209	1.1517	2.8405	1.25	0.3286	-23.453	5.61866	6

<sup>a</sup>Coefficients in Eqs. (3) and (4).

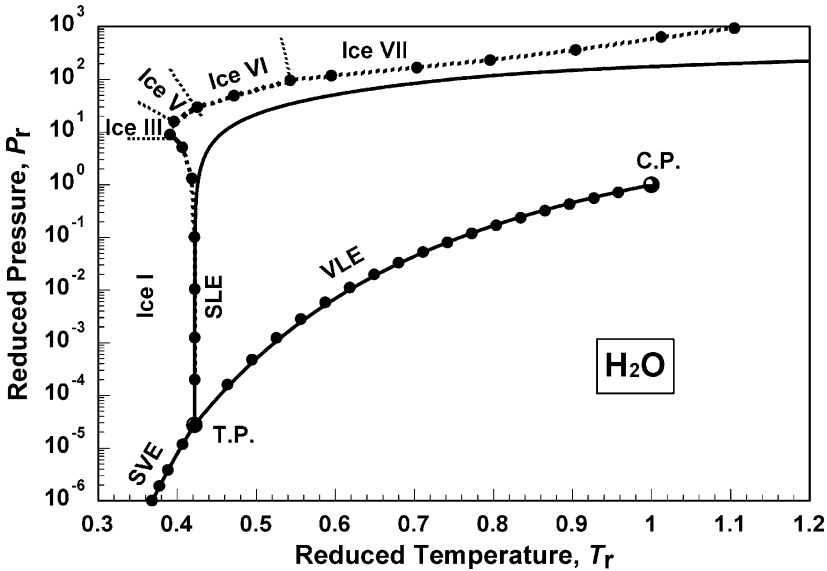


Fig. 1. Temperature–pressure phase diagram of water: SLE (solid–liquid equil.), SVE (solid–vapor equil.), and VLE (vapor–liquid equil.). Solid lines are calculated with the present unified solid–liquid–vapor EOS, and dotted lines and solid circles are taken from Refs. 37 and 38.

In terms of  $N$ -component mixtures, it can be written as

$$a = \sum_{i,j=1}^N \sqrt{a_i a_j} (1 - K_{ij}) x_i x_j, \quad (5)$$

$$K_{ij} \equiv \frac{k_{ij} k_{ji} (x_i + x_j)}{k_{ji} x_i + k_{ij} x_j}, \quad \text{and } K_{ii} = 0. \quad (6)$$

When  $k_{ij} = k_{ji}$  (symmetric), then it becomes the usual quadratic mixing in the mole fraction with  $K_{ij} = k_{ij}$ . Here, the binary interaction parameter  $k_{ij}$  can be a function of temperature if needed.

For the volumetric EOS parameters, we use simple molar averages of constituent molecules.

$$b = \sum_{i=1}^N b_i x_i, \quad c = \sum_{i=1}^N c_i x_i, \quad d = \sum_{i=1}^N d_i x_i \quad (7)$$

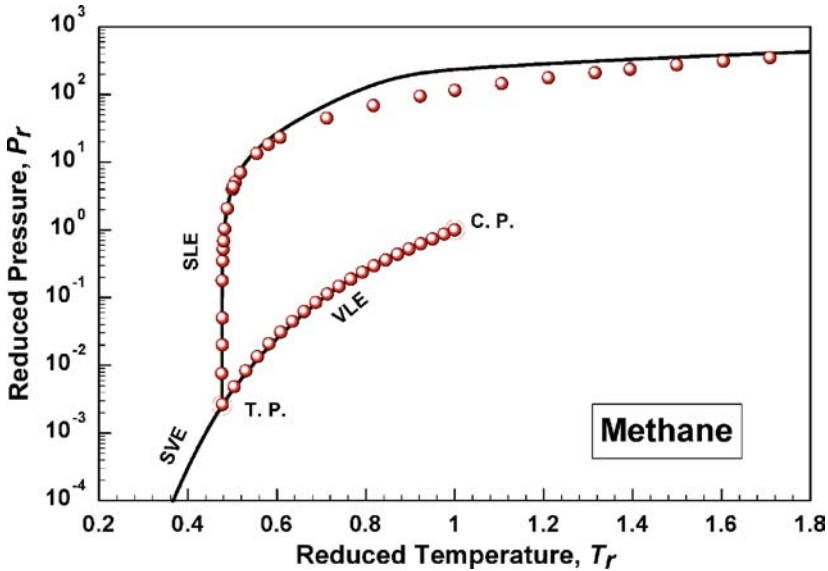


Fig. 2. Temperature–pressure phase diagram of methane: SLE (solid–liquid equil.), SVE (solid–vapor equil.), and VLE (vapor–liquid equil.). Solid lines are calculated with the present EOS, and symbols are taken from Ref. 39.

Thus, for binary mixtures, only two parameters  $k_{12}$  and  $k_{21}$  are required for the mixture EOS. Once we know these parameters, we can calculate all thermodynamic properties and phase behaviors of the mixture. In the present work, we are particularly interested in constructing and understanding three-phase equilibria (univariant states in a binary system), containing the solid state.

### 2.3. Hydrate (Clathrate) State

Gas hydrates (clathrates) are unique states of matter. They form solid-state crystals with well-defined crystal structures, often called Structure I, Structure II, or Structure H, *etc.*, depending upon the size of “guest” (gaseous) molecules or temperature–pressure conditions [7, 24–26]. However, it is known that the clathrate is not a stoichiometric true compound state, since the composition of the gaseous molecules in the clathrate varies with ( $T$ ,  $P$ ) conditions [7]. At the same time, it is not a simple solid-solution state. If it were a simple solid-solution state, the present EOS could be applied directly for the phase-behavior calculation, as demonstrated in the previous work on the solid state in methane–carbon dioxide binary mixtures [17]. If it were

a true compound, then we must have a pure compound EOS for the clathrate; the system becomes ternary mixtures of pure water, gaseous molecule and the clathrate compound. As long as the clathrate is not a stoichiometric pure compound, we could still treat the clathrate as a solid-solution state, but a “special (pseudo) solid-solution state”, and apply the present EOS as if it were a binary mixture system. This is the basis of the present clathrate modeling with the unified solid–liquid–vapor EOS.

Then, the question is how to model the special (pseudo) solid solution. First, we observe the fact that the clathrate can co-exist (be in phase equilibrium) with pure water ice as a distinctive state. This means that the water ice in the clathrate must be different from the pure water ice, and that the solid-state EOS for the clathrate-forming water must be modified accordingly. Physically, this situation makes sense, since if the same water solid exists in both the pure ice and clathrate ice, we cannot talk about the phase equilibrium between the two states: guest gaseous molecules can exist in both ices equally, and there are no two distinctive states!

Then, it is quite natural to imagine that the clathrate-forming ice has a larger specific volume than that of the pure ice in order to accommodate guest molecules in the hydrogen-bonded ice cage. Or, equivalently, we could imagine that the clathrate-forming ice has a weaker attractive interaction among water ice molecules than that in the pure ice. In terms of the present EOS modification for the clathrate-forming ice, the former case can be realized by increasing the EOS “*b*” parameter in Eq. (2) slightly with a modifying factor ( $c_b$ ): *i.e.*,  $b(\text{clathrate ice}) = b(\text{pure ice}) \times c_b$ . For the latter case, the water EOS “*a*” parameter in Eq. (2) can be reduced slightly with a modifying factor ( $c_a$ ): that is,  $a(\text{clathrate ice}) = a(\text{pure ice}) \times c_a$ . Such a hypothetical EOS for ice can only physically exist under the clathrate-forming state. The present idea about the clathrate-forming ice is exactly parallel with the traditional clathrate modeling [7], which assumes different forms for the pure ice and the clathrate ice that is unstable or meta-stable without guest molecules.

Secondly, another important observation in the present clathrate model with the EOS is as follows. If it is a unique solid solution, then we expect that the binary interaction parameters in the clathrate state will be unique and different from those in the liquid and/or vapor mixture states. If it is an ordinary simple solid solution like the methane-carbon dioxide case [17], the same single set of binary interaction parameters is sufficient to model all states (solid, liquid, and vapor mixture states). Thus, here we should have a set of the binary interaction parameters in the solid solution (clathrate) state, denoted as  $k_{12S}$  and  $k_{21S}$ , different from the liquid and vapor states, denoted as  $k_{12}$  and  $k_{21}$ .

### 3. ANALYSIS AND RESULTS

In the present clathrate model, four binary interaction parameters, ( $k_{12}, k_{21}, k_{12S}, k_{21S}$ ) and  $c_b$  (or  $c_a$ ), are required to describe the phase behavior of clathrates. However, the binary interactions are often temperature-dependent. In order to model the clathrate phase behavior in a wide temperature range, these interaction parameters themselves contain more adjustable parameters for the temperature dependence. The estimation of binary interaction parameters is made basically in the same way as the ordinary (fluid-only) EOS for mixtures; e.g., using VLE (vapor-liquid equilibrium),  $TPx$  (temperature-pressure-composition) data at some temperatures (or pressures). In the present methane-water system, among several experimental data [27–30], we have selected VLE data in Ref. 27, which were measured at low temperatures and moderate pressures below the gas hydrate forming conditions. Analyzing their VLE data at about 274.4 and 285.6 K, we have estimated the following interaction parameters,  $k_{12}$  and  $k_{21}$ , for methane (1)/water (2).

$$k_{12} = -1.5097 + 4.0579 \times 10^{-3} T[\text{K}] \quad (8)$$

$$k_{21} = -0.0245 \quad (9)$$

Calculated methane solubility curves with these parameters are compared in Fig. 3 with some experimental data. For the vapor and liquid states, we apply these parameters for the entire temperature range in the present binary system.

Concerning the clathrate-state (or solid-state) binary interaction parameters,  $k_{12S}$  and  $k_{21S}$ , we must have the EOS for the hypothetical (or meta-stable) clathrate-forming ice, before estimating them. As discussed earlier, modifying the present water EOS with  $c_b$  (or  $c_a$ ) can create such an EOS. We have examined several cases with different values in  $c_b$  (or  $c_a$ ). The larger the value in  $c_b$  (or the smaller the value in  $c_a$ ) results in the higher concentration of guest molecules (methane) in clathrates. This fact is consistent with a physical picture, since the larger specific volume of the hypothetical ice can accommodate more guest molecules in the ice cavity.

In addition, we have observed that both  $c_b$  and  $c_a$  can create the clathrate state practically in the same way, when their values are properly set. Thus, in this paper we discuss only the  $c_b$  case. It is known that the guest-molecule concentration in the Structure I clathrate (methane gas hydrates) is about 14.3 % (maximum: completely filled cavity case) [7]. Using this information, we arrived at a value in the  $c_b$  of 1.014 as a

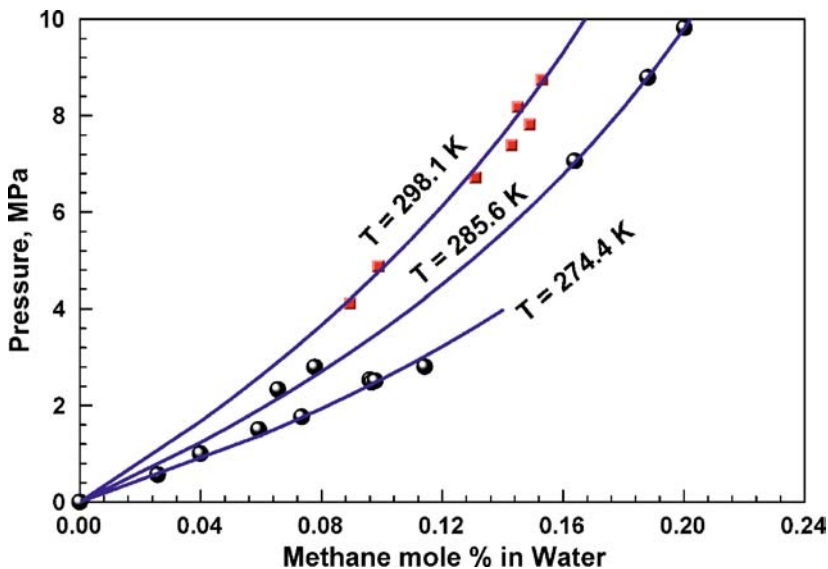


Fig. 3. Methane solubility (VLE) diagram at constant temperatures. Solid lines are calculated by the binary interaction parameters, Eqs. (8) and (9). Solid circles: experimental data [27], solid squares: selected experimental data [28].

reasonable one, after some trial-and-error analyses, although it is by no means a uniquely determined value. Here, we use this constant value *for the entire range of temperature and pressure conditions*, as far as the clathrate “ice” is concerned.

Then, using the  $c_b$  value of 1.014, the solid-state (clathrate-state) binary interaction parameters and their temperature dependence have been estimated by the use of selected three-phase (solid–liquid–vapor) equilibrium data.

Once these parameters are known, we can calculate a “complete” phase diagram of the three-phase equilibria using the present EOS model. Figure 4 shows the final result for a wide range of temperatures and pressures. In the following subsections, we will describe the detailed analyses and results in three ( $T, P$ ) regions separately: medium temperatures, low temperatures, and high temperatures/pressures.

### 3.1. Medium-Temperature Region

A temperature range from *c.a.* 270 to 320 K is characterized with the lower quadruple point (the invariant four-phases equilibrium: pure

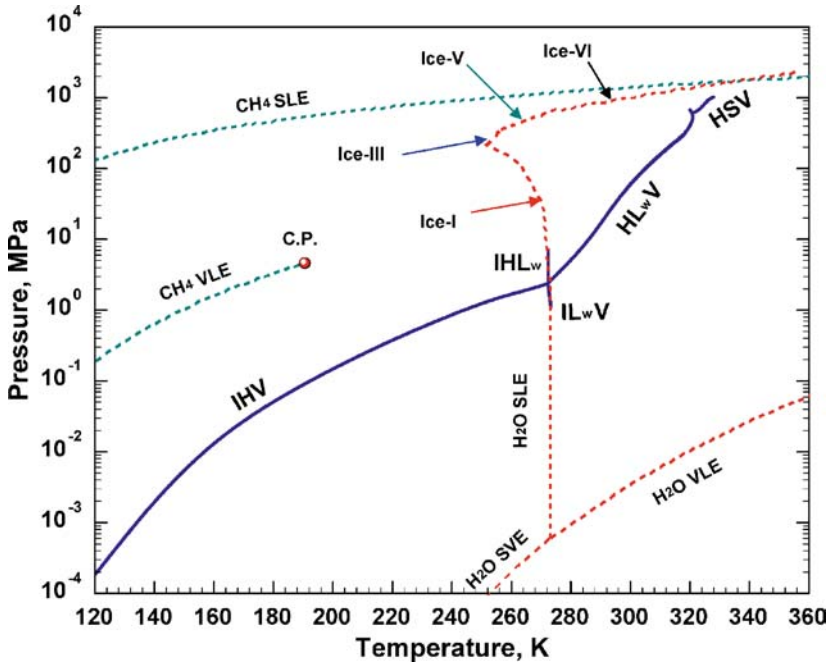


Fig. 4. Univariant three-phase lines for methane/water system. Solid lines: calculated by the present EOS model. IHV: ice/hydrate/vapor, HLwV: hydrate/water-rich liquid/vapor, ILwV: ice/water-rich liquid/vapor, IHLw: ice/hydrate/water-rich liquid, HSV: hydrate/solid solution/vapor. Phase behaviors of pure water [37, 38] and methane [39] are also shown with dotted lines.

ice/clathrate/water-rich liquid/methane-rich vapor), which we call  $Q_1$ , and the three-phase equilibrium of clathrate/water-rich liquid/methane-rich vapor (HLwV). In this work, we call methane “vapor”, although the proper name should be “fluid”, since methane is a supercritical fluid above 4.6 MPa in this temperature region; see Fig. 4. In order to estimate the clathrate-state (or solid-state) binary interaction parameters,  $k_{12S}$  and  $k_{21S}$ , we can use some of the HLwV data. Then, we have to solve the three-phase equilibrium conditions;

$$\phi_i^S x_i^S = \phi_i^L x_i^L = \phi_i^V x_i^V, \quad i = 1, 2 \quad (1 \text{ for methane and } 2 \text{ for water}), \quad (10)$$

where  $\phi$  is the fugacity coefficient of mixtures [17], superscripts, S, L, and V represent the solid (clathrate), liquid, and vapor phases, respectively, and each phase has the same temperature and pressure. Equation (10) is, however, a set of highly nonlinearly coupled equations, and the solution is

not straightforward without fairly accurate “initial” (guess) values in the Newton–Raphson method (or any nonlinear-equation solver). In addition, there are meta-stable and/or unstable states, which also satisfy Eq. (10).

There is a powerful and simple method to solve Eq. (10) for the true equilibrium condition, without making tedious iterative computations. It is called the “common-tangent method” in a Gibbs free energy plot as a function of composition at given  $T$  and  $P$  [16, 31, 32]. We can visually observe the phase equilibrium condition on the graphical plot (or on a computer screen). The dimensionless Gibbs free energy for an  $\alpha$  ( $=$  S, L, or V) state is given by

$$\frac{G^\alpha}{RT} = x_1^\alpha \left( \ln(Px_1^\alpha) + \ln\phi_1^\alpha - \ln\phi_1^0 \right) + x_2^\alpha \left( \ln(Px_2^\alpha) + \ln\phi_2^\alpha - \ln\phi_2^0 \right), \quad (11)$$

where  $\phi_i^0$  is a reference-state fugacity coefficient, which was chosen here as the pure solid state of  $i$ th species at the system  $T$  and  $P$ , although the reference state is not important in the common-tangent method.

We have used this method extensively to understand the physical meaning of phase behaviors and to estimate the binary interaction parameters. A typical example of the Gibbs free-energy plot is shown in Fig. 5. The estimation of the clathrate-state (or solid-state) binary interaction parameters,  $k_{12S}$  and  $k_{21S}$ , and their temperature dependence has been made using this graphical method with several trial-and-error analyses of four experimental data points (at 318.4 K [18], 301.6 K [33], 285.7 K [34], and the  $Q_1$  point of 272.29 K). The temperature and pressure of the  $Q_1$  point was estimated from the crossing point of experimental HLwV data [34] and IHV (pure ice/clathrate/vapor) data [35]:  $T_{Q_1} = 272.29$  K and  $P_{Q_1} = 2.387$  MPa. Then, we obtain the following interaction parameters in this temperature region, methane (1)/water (2) binary system.

$$k_{12S} = -1.2263 + 0.80916\tau + 3.3596\tau^2 + 5.1937\tau^3, \quad (12)$$

where  $\tau = T[K]/100 - 2.9450$ .

$$k_{21S} = -0.40 \quad (13)$$

It should be mentioned that  $k_{21S}$  was found to be a quite insensitive parameter for the HLwV phase behavior in the present temperature range. Thus, we treated it as a constant. This insensitivity in  $k_{21S}$  can be easily understood from Fig. 5. Since  $k_{21S}$  controls mainly the shape of the solid Gibbs energy near the methane-rich side and the Gibbs energy of the pure solid methane is far from that of the pure vapor, the methane-rich-side solid does not play any significant role for the present phase equilibrium (or does

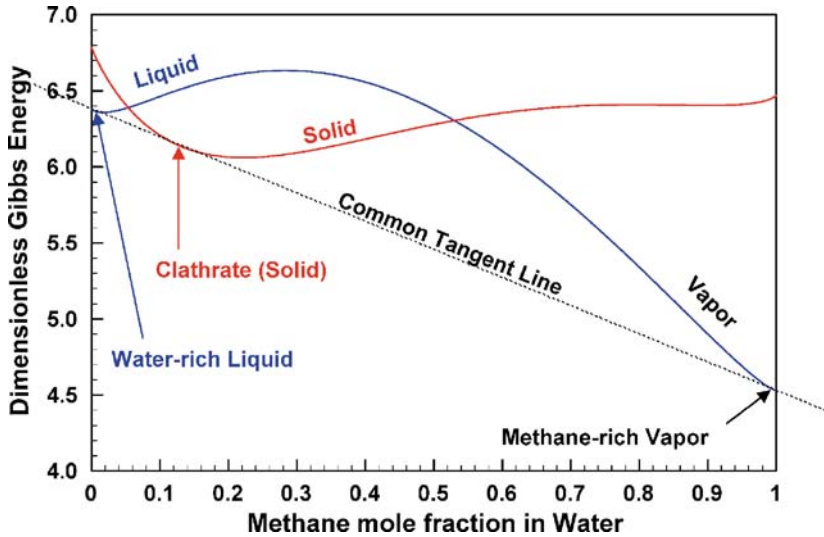


Fig. 5. Gibbs free energy plot of methane-water mixtures for a HLwV data point at  $T=301.6$  K and  $P=65.4$  MPa [33]. A common-tangent line for the three-phase (solid–liquid–vapor) equilibrium can be drawn with proper binary interaction parameters in the solid state (see text):  $k_{12S}=-1.15$  and  $k_{21S}=-0.40$  for methane (1) and water (2). The interaction parameter  $k_{12S}$  determines the shape of the solid Gibbs energy near the water-rich side, while  $k_{21S}$  controls the shape of the solid Gibbs energy near the methane-rich side.

not intervene in other phase states). However, this situation changes under high pressures; see Subsection 3.3.

A three-phase HLwV diagram calculated with these binary interaction parameters is shown in Fig. 6, compared with experimental data. The predicted curve with these interaction parameters represents the observed data quite well. Figure 7 shows the calculated methane composition in each phase along the HLwV line.

In addition, using the interaction parameters from Eqs. (12) and (13), we have predicted other three-phase equilibrium curves in the present temperature region: pure ice/hydrate/methane-rich vapor (IHV), pure ice/water-rich liquid/methane-rich vapor (ILwV), and pure ice/hydrate/water-rich liquid (IHLw), which are also shown in Fig. 6. The branching behavior of three-phase lines around the  $Q_1$  point is essentially the same as the commonly known type. However, the behavior of the IHLw line at high pressures is quite unexpected. The line becomes bent over and meets the HLwV line again, forming the second quadruple point ( $Q_2$ : IHLwV) at 314 K and 216.2 MPa. Then, careful investigations revealed that the stable

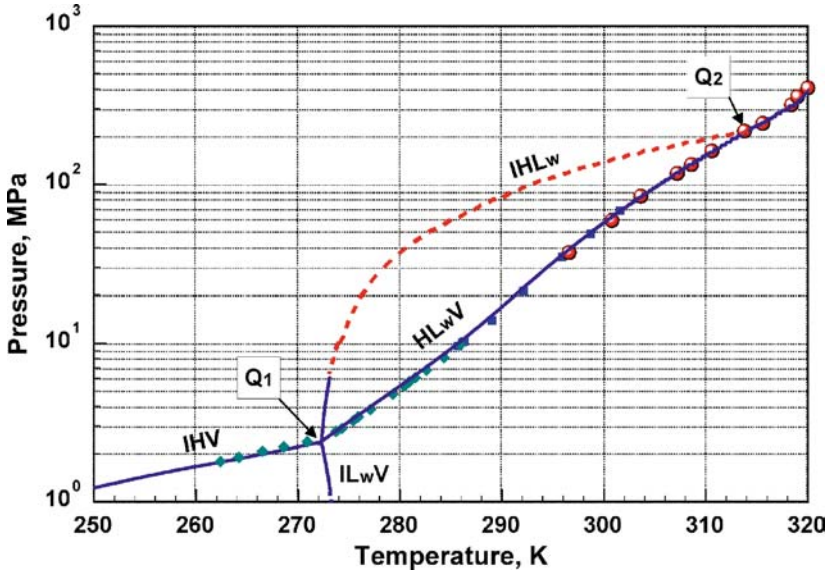


Fig. 6. Three-phase lines at medium temperatures: see text for details. Solid and dotted lines are calculated by the present EOS model, and various symbols are experimental data taken from different authors [24].

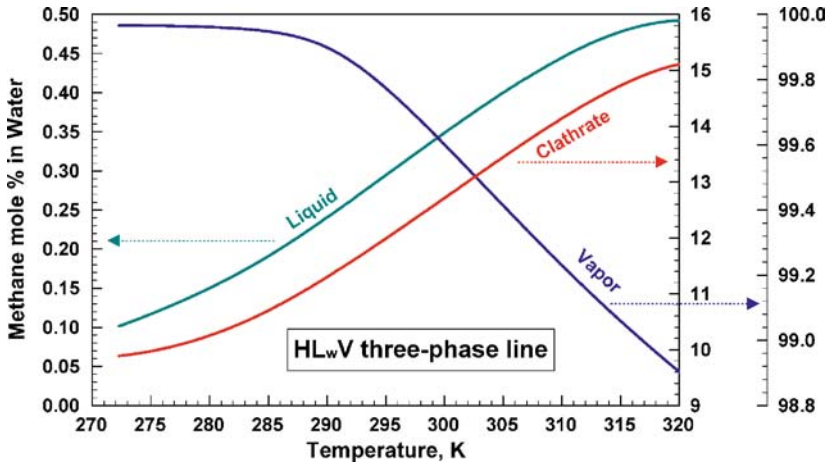


Fig. 7. Calculated methane compositions in water along the three-phase HLwV line of Fig. 6.

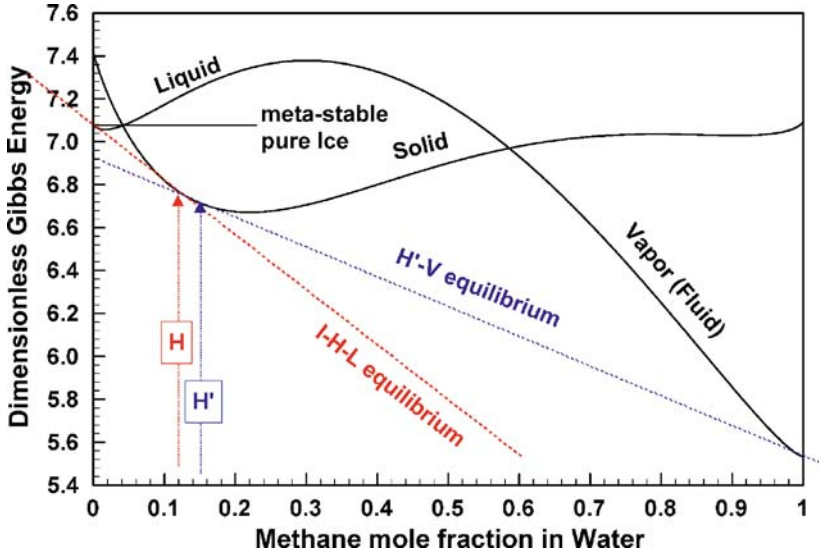


Fig. 8. Gibbs free energy plot of methane-water mixtures with metastable ice at  $T=300\text{ K}$  and  $P=139\text{ MPa}$  in the IHLw line of Fig. 6: see text for details.

pure ice in this line exists only under *c.a.*  $6\text{ MPa}$  ( $T \leq 273.15\text{ K}$ ), and above this pressure and temperature, the ice becomes metastable (superheated) ice. Thus, at the higher-pressure region in this line, the calculated IHLw phase will be metastable three-phase equilibria: *metastable pure ice/hydrate/water-rich liquid*. Also, at this three-phase equilibrium ( $T$ ,  $P$ ) condition, there always exist stable two-phase (*another hydrate/methane-rich vapor*) equilibria, as shown in Fig. 8 as a typical example. It is, however, conceivable that the *metastable ice* can be stabilized by the presence of the hydrate ice, and this IHLw line may be a true stable three-phase line. This intriguing thought will be further discussed in Section 4.

The calculated ILwV line is stable above about  $P = 1.18\text{ MPa}$  and below  $T = 273.15\text{ K}$ , where the stable pure ice exists. In this case, the metastable ice would not be stabilized by the coexisting liquid and vapor phases. Concerning the IHV three phases, further details are given in the following subsection.

### 3.2. Low-Temperature Region

At temperatures below the  $Q_1$  point ( $272.29\text{ K}$ ), there exists the three-phase line of pure water ice (Ice I)/clathrate/methane-rich vapor states. The binary interaction parameters of Eqs. (12) and (13) were able to predict

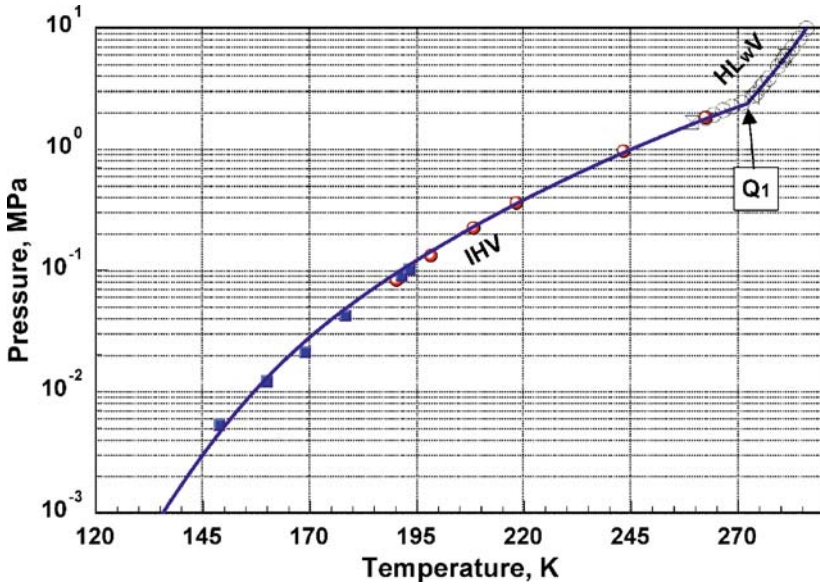


Fig. 9. Three-phase (IHV: ice/hydrate/vapor) line at low temperatures. Solid line: calculated. Various symbols: experimental data from different sources [24, 35, 36].

such a line. However, below about 260 K, the predicted pressure became underestimated with respect to the experimental values [35, 36]. This is not surprising, since we are using the extrapolated values in the empirical  $T$ -dependent function Eq. (12). In principle, it is possible to modify Eq. (12) so as to reproduce the low temperature data as well. However, the  $T$ -dependent function would become highly complex. Thus, we use a piece-wise continuous function for  $k_{12S}(T)$ . Estimating  $k_{12S}$  values from experimental data [35, 36] around 200 and 160 K and using the value in Eq. (12) at 260 K, we obtain the following equations: here  $k_{21S}$  was assumed to be the constant in Eq. (13).

$$k_{12S} = -1.27801 - 0.18201\tau + 0.19778\tau^2, \quad (14)$$

where  $\tau = T[\text{K}]/100 - 2.0667$ , and  $T \leq 260$  K.

The low-temperature three-phase line has been calculated with these interaction parameters. Figure 9 shows the result, compared with the available experimental data [35, 36]; the calculated line represents the observed data quite well. The methane compositions in clathrate and vapor phases along the IHV line are shown in Fig. 10.

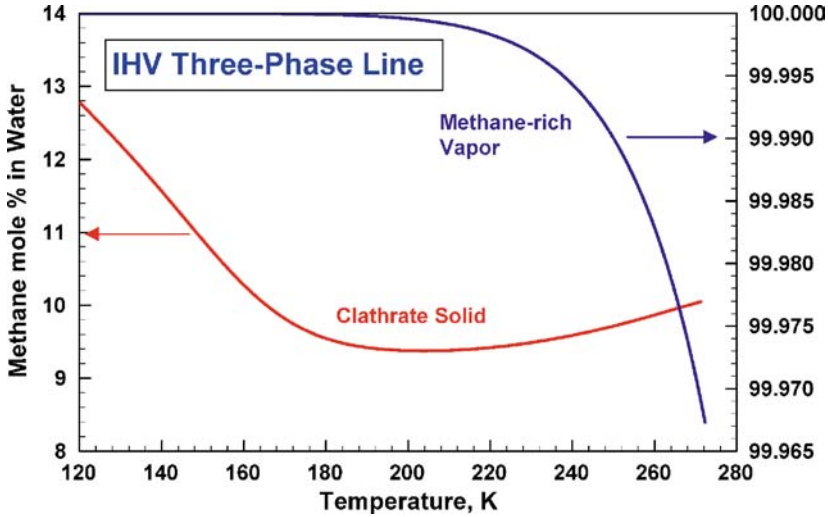


Fig. 10. Calculated methane compositions in water along the IHV line in Fig. 9.

### 3.3. High-Pressure Region

A region of temperatures above *c.a.* 320 K and pressures above *c.a.* 400 MPa presents highly complex features. Experimental data [18] show quite unusual behaviors, having the temperature maximum around 320.9 K, high pressure slopes within a very narrow temperature range, metastable states, and an upper quadruple point ( $Q_3$ ). Dyadin et al. [18] suggested that a new form of solid (clathrate) appears in this high-pressure region, and the new form would not be the Structure II methane hydrate, as one might guess. Indeed, Hirai et al. [19] experimentally observed that at 1500 MPa methane hydrate partially decomposed to ice VI and liquid methane, and that the remaining methane hydrate kept Structure I even at this very high pressure. However, Chou et al. [20] claimed that the Structure II and Structure H clathrates occur as well as the Structure I in high-pressure regions.

Therefore, we have examined extensively the phase behaviors in these ( $T, P$ ) regions using the Gibbs-free energy plot, mentioned before. It has been found that the three-phase equilibrium cannot be uniquely identified, particularly for the region with the high-pressure slope ( $320.0 \text{ K} < T < 320.9 \text{ K}$ ). This is because the Gibbs energies (solid and liquid of water, or solid and vapor of methane) in both of the pure-component sides become closer and start to intervene with each other. Both interaction parameters,  $k_{12S}$  and  $k_{21S}$ , become important and start coupling with each other.

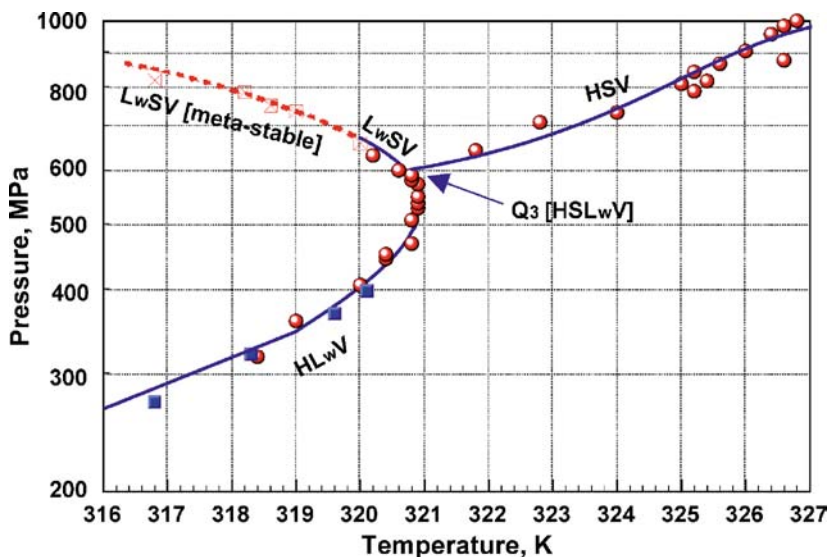


Fig. 11. Three-phase diagram at high-pressure regions. Solid and dotted lines are calculated by the present EOS model: see text for details. Solid circles and open squares: experimental data [18]; solid squares: experimental data [33].

By changing these parameters, we can create different types of three-phase equilibria, particularly in the high-pressure slope area mentioned above. Although the situation is complicated and ambiguous, there exist some constraints: the existence of the  $Q_3$  point and a high pressure phase-equilibrium condition near 1000 MPa. With these constraints and the information available, we have modeled the phase behavior in the present ( $T$ ,  $P$ ) region, and the calculated phase behavior is shown in Fig. 11, and compared with the observed data [18]. We will describe some details about the present model below.

First, we have looked at an observed three-phase point at  $T=326.8$  K and  $P=1000$  MPa [18], for which Dyadin et al. suggest a “novel” hydrate (different from the Structure I hydrate but not a Structure II hydrate) that coexists with water-rich liquid and methane-rich vapor [18]. Our Gibbs free-energy analysis is shown in Fig. 12. One can easily guess from Fig. 12 what kind of three-phase equilibria can possibly occur. The relative Gibbs energy in solid, liquid, and vapor states of both pure compounds is fixed at the given temperature and pressure. Then, Fig. 12 predicts the possible three-phase equilibrium, without having a precise knowledge of the binary interaction parameters, even though they can change the shape of the Gibbs energy curves. Based on the methane composition in the

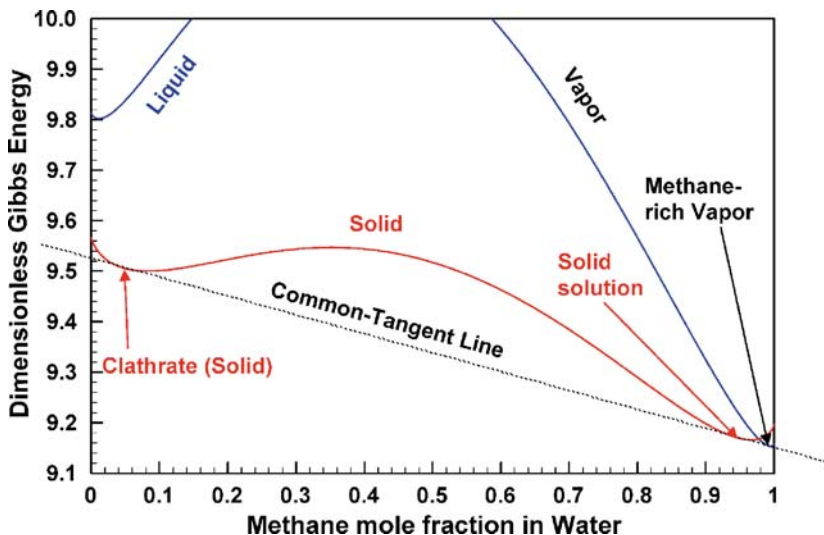


Fig. 12. Gibbs free energy plot for the HSV three-phase line (Fig. 11) at  $P = 1000$  MPa and  $T = 326.8$  K (observed data point [18]).

mixture, the three phases are clearly the “Structure I” clathrate, methane-rich vapor, and methane-rich solid, which would not be a new clathrate (“novel” hydrate) but likely be just a solid solution of methane and water.

Thus, the three-phase equilibrium in this region is called “HSV” (hydrate-solid solution-vapor). The binary interaction parameters for the HSV line were estimated from three data points (at about 326, 324, and 321 K);

$$k_{12S} = -0.414 \quad (15)$$

$$k_{21S} = -0.53424 + 5.3535\tau + 54.453\tau^2, \quad (16)$$

where  $\tau = T[K]/100 - 3.2362$ , and  $T \geq 320$  K. It should be noted that we have treated  $k_{12S}$  as a constant for simplicity, since in this region  $k_{21S}$  (methane-rich-side parameter) only plays the major and sensitive role for the three-phase equilibrium, as one could imagine from Fig. 12.

Secondly, we have looked at the upper quadruple point ( $Q_3$ ), which was estimated from the crossing point of two experimental three-phase curves [18]:  $T \approx 320.85$  K and  $P \approx 590$  MPa. Using this temperature and pressure, the Gibbs energy plot with the common-tangent method has been examined to determine the existence of any quadruple-point phase equilibrium. The upper quadruple-point equilibrium ( $Q_3$ ) can be created

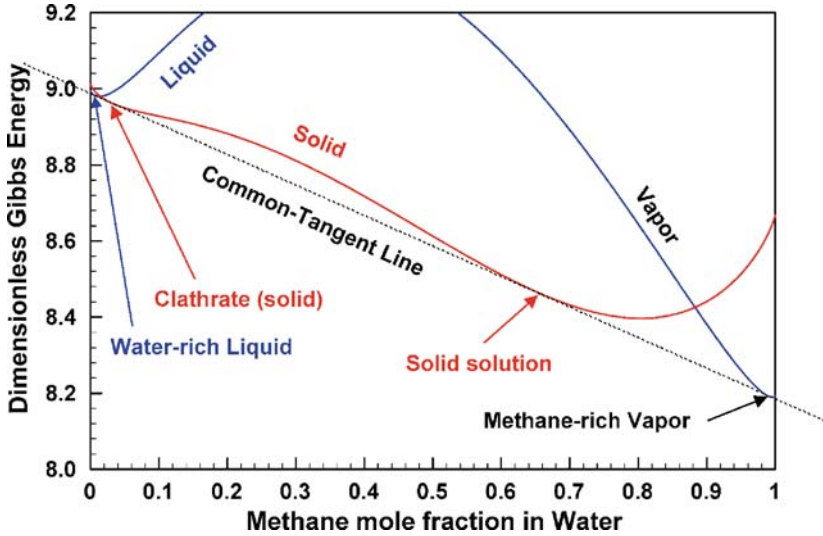


Fig. 13. Gibbs free energy plot for the upper quadruple point ( $Q_3$ ) reported in Ref. 18.

with the interaction parameters of  $k_{12S} = -0.414$  and  $k_{21S} = -0.6715$ , which is reasonably close to  $k_{21S} = -0.6408$  from Eq. (16), and is shown in Fig. 13. In the present model, the  $Q_3$  point is found to be an equilibrium state of water-rich liquid/clathrate/solid solution/methane-rich vapor: “HLwSV” state.

Thirdly, we have examined the observed metastable data [18] (about  $317\text{ K} < T < 320\text{ K}$ , and  $P >$  about  $650\text{ MPa}$ ) to understand what kind of three-phase metastable states could exist. Figure 14 shows the Gibbs-energy analysis for an experimental metastable state at  $T = 320\text{ K}$  and  $P = 658\text{ MPa}$  [18], which is located near the  $Q_3$  point. It can be seen from Fig. 14 that the three-phase metastable state consists of a water-rich liquid, solid solution, and methane-rich vapor: “LwSV” state. Another metastable common-tangent line can be drawn for the hydrate and solid solution, which is a two-phase metastable state. A stable common-tangent line also exists in this figure, although it is not shown, which is a two-phase equilibrium between the hydrate and methane-rich vapor. In addition, we have found that this three-phase (LwSV) metastable state becomes stable as the temperature and pressure approach the  $Q_3$  point and below the quadruple-point pressure. This is because the liquid Gibbs energy in the pure-water side becomes smaller than the solid Gibbs energy with a decrease in pressure, and then the stable LwSV results; refer to Fig. 14. Using a trial-and error method, these LwSV states were modeled by the

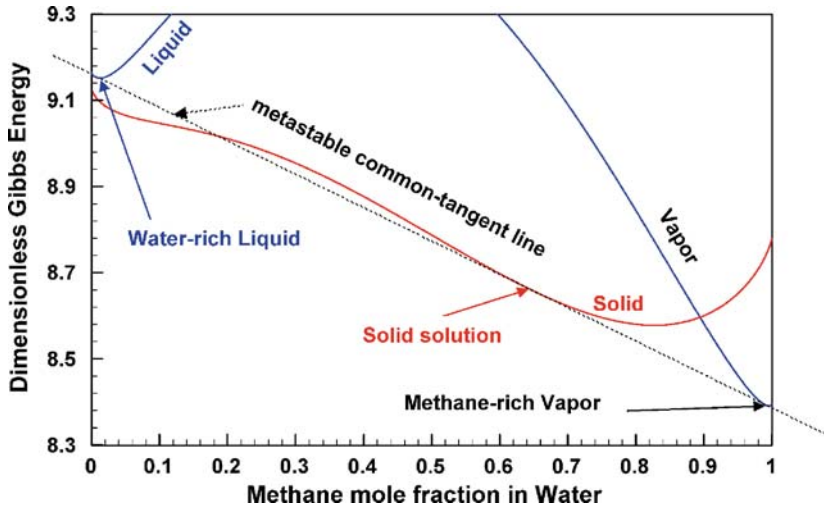


Fig. 14. Gibbs free energy plot for an observed metastable three-phase state at  $T = 320$  K and  $P = 658$  MPa [18] in the dotted line of Fig. 11.

following binary interaction parameter with the same  $k_{12S} = -0.414$  as Eq. (15):

$$k_{21S} = -0.7688 + 0.1950 \times (320.90 - T)^{0.43}, \quad (17)$$

for  $T \leq 320.90$  K and  $P \geq 526$  MPa.

Finally, we have investigated how the HLwV line (Subsection 3.1) approaches the  $Q_3$  point within a narrow temperature interval of about 0.9 K (320 to 320.9 K) and with high-pressure variations. With the interaction parameters used in the HLwV line of Subsection 3.1, Eqs. (12) and (13) cannot correlate the observed behavior. Therefore, we have developed new interaction parameters in this region, based on the Gibbs-energy plot analysis;

$$k_{12S} = -0.5261 - 0.1564 \times (320.90 - T)^{0.48}, \quad (18)$$

for  $319.0 \leq T \leq 320.90$  K and  $P \leq 526$  MPa, while  $k_{21S}$  was assumed to be the same as Eq. (13). Equation (18) is a piece-wise continuation of Eq. (12) for the HLwV phase behavior at  $T = 319.0$  K, and was estimated by a trial-and-error method.

A three-phase diagram for the high-pressure and -temperature region has been constructed with the above interaction parameters, and is shown in Fig. 11, and compared with available experimental data [18, 33].

#### 4. DISCUSSION

In this report, we have improved our proposed method for clathrate modeling [16], which is a completely new approach and different from the traditional model: the statistical thermodynamic model by van der Waals and Platteeuw [7] and its many improved variants [8–15]. The present model is an attempt to describe all thermodynamic states (solid (clathrate), liquid, and vapor) consistently with a single unified solid–liquid–vapor EOS. This is only possible when we have such a unified solid–liquid–vapor EOS [17]. In general, an EOS only describes the state of matter (solid, liquid, or vapor), and does not reveal any micro-structures in fluid and solid, or solid crystal modifications, except for the mixture composition. However, there are some advantages, such as classifying the phase behaviors in a thermodynamically consistent way for solid, liquid, and vapor states. The present EOS method is also conceptionally simple. Equilibrium calculations including solid states are just the same as the familiar VLE, LLE, or VLLE calculations with usual fluid-only EOS (e.g., PR or SRK types of EOS). However, since clathrates (hydrates) are not simple solid solution, some special treatments for the clathrate state are required, as discussed in Section 2.3.

Using the present improved model, we have analyzed the methane-hydrate (clathrate) phase behavior. Under medium and low pressures, the phase behaviors of clathrates were well modeled with the present EOS, and the three-phase equilibrium calculation was also straightforward. The methane concentration in clathrate (hydrate) varies, and the magnitude seems quite reasonable as the Structure I hydrate, as shown in Figs. 7 and 10. However, we have predicted an interesting and curious three-phase line IHLw (pure ice/hydrate/water-rich liquid), starting from the  $Q_1$  point; see Fig. 6.

Above *c.a.* 6 MPa along the IHLw line, pure ice becomes metastable (superheated), and thus the IHLw line would be in metastable three-phase equilibrium. In addition, when the methane *feed* composition is high, there exists another hydrate ( $H'$ ) along the IHLw ( $T, P$ ) line as the stable two-phase equilibrium:  $H'-V$ , as illustrated in Fig. 8. Concerning the metastable ice, it may be stabilized with help of the coexisting clathrate (hydrate) *ice*, and then the metastable IHLw line could be in thermodynamically stable three-phase equilibrium. The situation is similar to the case of the metastable “empty lattice” of hydrate in the traditional theory, which is stabilized with only the existence of guest molecules. This IHLw line becomes bent over with an increase in pressure, and then crosses the HLwV three-phase line, creating another quadruple point  $Q_2$  (IHLwV) around  $T=314$  K and  $P=216.2$  MPa; see Fig. 6. Another hydrate  $H'$  in the

stable two-phase  $H'$ - $V$  equilibria along the  $ILwV$  ( $T, P$ ) line becomes  $H$  at the  $Q_2$  point, and thus there is no quadruple point like  $HH'LwV$ .

This new  $Q_2$  is not well established or well known in the literature, except for Ref. 20, where they claim the existence of  $Q_2$ , although their interpretation of the quadruple point is different from the present study. They claim that the  $Q_2$  is composed of  $HH''LwV$  at  $T \approx 308$  K and  $P \approx 141$  MPa, where  $H$  is the Structure I hydrate and  $H''$  is the Structure II hydrate. Another difference between our  $Q_2$  and theirs [20] is that our  $Q_2$  point temperature (and pressure) is predicted to be higher by several degrees. This is due to the inaccuracy in the present water EOS for pure ice at high pressures, as clearly seen in Fig. 1. Therefore, our predicted  $Q_2$ -point temperature and pressure should be regarded as being semi-quantitative.

Phase behaviors of methane hydrates in high-pressure regions are quite complex, as mentioned in Section 3.3. So far, to the best of our knowledge, there is no clathrate modeling work in this pressure region, except for a partial modeling by Ballard and Sloan [9]. Their model is an extended modification of the statistical thermodynamic model of clathrates by van der Waals and Platteeuw [7]. Although their model predicts the maximum temperature around 320 K and the bending-over behavior of the  $HLwV$  line, it seems that they assumed the bending-over region to be stable  $HLwV$  phases, in spite of the experimentally known metastable states of undefined hydrate three phases [18]. Furthermore, it seems that their model did not predict the high-pressure quadruple point  $Q_3$  [18].

Like the quadruple point  $Q_2$ , the  $Q_3$  point is also not well defined and unfamiliar in the literature. One of the unsettled problems in high-pressure regions [18–21] is whether any new forms of hydrates appear and what they are: Structure II, other type of clathrate, or solid solution. We have examined these high-pressure regions with the Gibbs energy plot, based on the present unified EOS model. Figures 12 to 14 clearly show the appearance of a new form of solid state, which is a methane-rich solid (solid solution) and does not seem to be the clathrate hydrate. The appearance of this solid solution is due to the fact that the Gibbs energies of the solid and liquid of pure methane become closer to each other with an increase in pressure; see Figs. 12 to 14.

Finally, we have been able to model the  $Q_3$  point, the bending-over metastable three phases and other three-phase lines, as summarized in Fig. 11. Although the present results are still tentative due to both the inaccuracy of the EOS for the water ice state at high pressures and the limited use of available experimental data, our interpretation will be at least qualitatively correct and shed some light on the unsettled problem.

## 5. CONCLUSIONS

Our previously proposed model for the clathrate phase behavior has been refined and applied successfully to methane gas hydrates. The present model is thermodynamically fully consistent when dealing with the clathrate (solid), because of the unified solid–liquid–vapor EOS. The solid state can be treated equivalently as just another state of matter, like liquid or vapor.

Although the EOS model cannot describe the details of crystal modifications and micro-structures of the solid state, the information of the mixture composition gives us a useful idea about the clathrate state and structure. Furthermore, the EOS model has an advantage in understanding the global phase transition behavior in a consistent way.

Highly complex behaviors and unknown solid states at high-pressure regions have been modeled for the first time. The present interpretation of these areas may help the further understanding of complex behaviors of methane gas hydrates.

## 6. ACKNOWLEDGMENTS

The author thanks Dr. G. K. Anderson at Los Alamos National Laboratory for informing the author about Refs. 18, 19, and 20, which were highly important in the present study of the high pressure region data. Also, the author appreciates Dr. E. D. Sloan Jr. at Colorado School of Mines for his comment on a new phase or something interrupting the HLwV equilibria around and above 320 K, and for his encouragement on the present clathrate modeling.

## REFERENCES

1. M. D. Max, ed., *Natural Gas Hydrate: In Oceanic and Permafrost Environments* (Kluwer Acad. Pub., London, 2000).
2. M. D. Max and A. Lowrie, *J. Petrol. Geol.* **19**:41 (1966).
3. P. G. Brewer, C. Friederich, E. T. Peltzer, and F. M. Orr, *Science* **284**:943 (1999).
4. P. G. Brewer, F. M. Orr, G. Friederich, K. A. Kvenvolden, and D. L. Orange, *Energy and Fuels* **12**:183 (1998).
5. S. Kikuchi and H. Ono, Japanese Patent (JP2003139357 A) (2003).
6. M. D. Max and R. E. Pellenbarg, U.S. Patent (No. 5,873,262) (1999).
7. J. H. van der Waals and J. C. Platteeuw, *Adv. Chem. Phys.* **2**:1 (1959).
8. W. R. Parrish and J. M. Prausnitz, *Ind. Eng. Chem. Proc. Des. Dev.* **11**:26 (1972).
9. A. L. Ballard and E. D. Sloan Jr., *Fluid Phase Equilib.* **194–197**:371 (2002).
10. J. B. Klauda and S. I. Sandler, *Ind. Eng. Chem. Res.* **39**:3377 (2000).
11. J. B. Klauda and S. I. Sandler, *J. Phys. Chem. B.* **106**:5722 (2002).
12. J. B. Klauda and S. I. Sandler, *Chem. Eng. Sci.* **58**:27 (2003).

13. S. O. Yang, S. H. Cho, H. Lee, and C. S. Lee, *Fluid Phase Equilib.* **185**:53 (2001).
14. G.-J. Chen and T.-M. Guo, *Fluid Phase Equilib.* **122**:43 (1996).
15. J.-H. Yoon, Y. Yamamoto, T. Komai, and T. Kawamura, "PSRK Group Contribution Method for Predicting Phase Equilibria of Gas Hydrate," *Proc. 15th Symp. Thermophys. Properties*, June 22–27, Boulder, Colorado (2003).
16. A. Yokozeki, *Fluid Phase Equilib.* **222–223**:55 (2004).
17. A. Yokozeki, *Int. J. Thermophys.* **24**:589 (2003).
18. Y. A. Dyadin, E. Ya. Aladko, and E. G. Larinov, *Medeleev Commun.* **7**:34 (1997).
19. H. Hirai, T. Kondo, M. Hasegawa, T. Yagi, Y. Yamamoto, T. Komai, K. Nagashima, M. Sakashita, H. Fujihisa, and K. Aoki, *J. Phys. Chem. B* **104**:1429 (2000).
20. I. Chou, A. Sharma, R. C. Burruss, H. Mao, R. J. Hemley, A. F. Goncharov, L. A. Stern, and S. H. Kirby, *Proc. Natl. Acad. Sci.* **97**:13484 (2000).
21. J. S. Loveday, R. J. Nelmes, M. Guthrie, S. A. Blemonte, D. R. Allan, D. D. Klug, J. S. Tse and Y. P. Handa, *Nature* **410**:661 (2001).
22. A. Yokozeki, *Int. J. Thermophys.* **22**:1057 (2001).
23. R. Stryjek and J. H. Vera, *Can. J. Chem. Eng.* **64** (1986) 820.
24. E. D. Sloan Jr., *Clathrate Hydrates of Natural Gases*, 2nd Ed. (Marcel Dekker, New York, 1998).
25. T. C. W. Mak and R. K. McMullen, *J. Chem. Phys.* **42**:2732 (1965).
26. J. A. Rimeester, J. S. Tse, C. I. Ratcliffe, and B. M. Powell, *Nature* **325**:135 (1987).
27. K. Lekvam and P. R. Bishnoi, *Fluid Phase Equilib.* **131**:297 (1997).
28. K. Y. Song, G. Feneyrou, F. Fleyfel, R. Martin, J. Lievois, and R. Kobayashi, *Fluid Phase Equilib.* **128**:249 (1997).
29. P. Servio and P. Englezos, *J. Chem. Eng. Data* **47**:87 (2002).
30. A. Chapoy, C. Coquelet, and D. Richon, *Fluid Phase Equilib.* **214**:101 (2003).
31. C. H. P. Lupis, *Chemical Thermodynamics of Materials* (North-Holland, New York, 1983).
32. A. Yokozeki, *Int. J. Thermophys.* **25**:643 (2004).
33. D. R. Marshall, S. Saito, and R. Kobayashi (1964), cited in Ref. 24.
34. S. Adisasmito, R. J. Frank, and E. D. Sloan, *J. Chem. Eng. Data* **36**:68 (1991).
35. T. Y. Makogon and E. D. Sloan, Jr., *J. Chem. Eng. Data* **39**:351 (1994).
36. B. J. Felabella (1975), cited in Ref. 26.
37. W. Wagner, A. Saul, and A. Pruß, *J. Phys. Chem. Ref. Data* **23**:515 (1994).
38. W. Wagner and A. Pruß, *J. Phys. Chem. Ref. Data* **31**:231 (2002).
39. U. Setmann and W. Wagner, *J. Phys. Chem. Ref. Data* **20**:1061 (1991).